JOURNAL OF MATERIALS SCIENCE 32 (1997) 2855–2871

The lateral deformation of cross-linkable PPXTA fibres

M. C. G. JONES*, E. LARA-CURZIO§, A. KOPPER, D. C. MARTIN‡
Department of Materials Science and Engineering and the Macromolecular Science and Engineering Center, The University of Michigan, 2022 H. H. Dow Building, Ann Arbor, MI 48109-2136 USA §*High Temperature Materials Laboratory, Bldg. 4515, Oak Ridge National Laboratories, PO Box 2008, Oak Ridge, TN 37831-6062, USA*

The lateral deformation properties of oriented polymer fibres were examined by transverse compressive and torsional experiments. A modified interfacial test system machine was used to study the transverse compressive deformation behaviour of thermally cross-linkable poly(*p*-1,2-dihydrocyclobutaphenylene terephthalamide) (PPXTA) fibres and of a number of commercially available polymers (Nomex, nylon, Kevlar, Dacron) and ceramic (Nicalon and FP) fibres. The torsional (shear) modulus *G* of PPXTA and Kevlar poly(*p*-phenylene terephthalamide) (PPTA) fibres was measured by pendulum experiments. During both fibre torsion and transverse compression, the deformation involves materials slip on (*hk*0) planes, in the [0 0 1] direction for the torsion and the [*hk*0] directions for transverse compression. The intermolecular crosslinks in PPXTA did not significantly modify the elastic transverse modulus E_t and caused only slight (13%) increase in shear modulus *G*. However, the plastic transverse properties of cross-linked PPXTA were significantly different than those of uncross-linked PPXTA. The stress at the proportional limit $\bar{\sigma}_p$, determined from the transverse load–displacement curves, was substantially higher for the cross-linked fibres than for the uncross-linked fibres. In addition, the cross-linked PPXTA fibres exhibited a large strain recoverable response reminiscent of elastomers, whereas the PPTA and uncross-linked PPXTA fibres exhibited a large strain irreversible response.

1. Introduction

Oriented extended-chain liquid crystalline fibres are composed of macromolecules almost perfectly oriented parallel to the fibre axis. Typically, the morphology is viewed as a set of long microfibrils oriented in the fibre axis direction, and containing crystallites separated by grain boundaries of oriented polymer. Thus, a given molecule (length $\approx$100 nm) will traverse many crystallites (size $\approx$10 nm) and possibly several microfibrils (lateral size $\approx$30 nm). Oriented extended-chain fibres are very stiff and strong when deformed in tension (tensile modulus $\approx$ 100 to 350 GPa; tensile strength $\approx$2 to 3.5 GPa) [1] but much weaker when deformed in compression, with the compressive strength typically one-tenth of the tensile strength [2]. This imbalance in mechanical properties results from the structural anisotropy. Whereas the axial tensile properties predominantly depend on the covalent bonds within the polymer backbone, the axial compressive properties depend more on the weaker secondary intermolecular bonds. Therefore, it is important to characterize the lateral deformation properties which depend on this secondary intermolecular bonding, e.g. the shear and transverse deformation properties.

The object of this study is to characterize the lateral deformation behaviour of cross-linkable poly(*p*-1,2-dihydrocyclobutaphenylene terephthalamide) (PPXTA) fibres and of poly(*p*-phenylene terephthalamide) (PPTA, tradename Kevlar) fibres. Thus, the longitudinal shear modulus (torsional modulus) and the compressive transverse properties of PPTA and of PPXTA are determined. Intermolecular cross-links may be induced in the extended-chain PPXTA fibre by choosing an appropriate heat treatment temperature. It is expected that the cross-linked PPXTA may have improved lateral properties compared to uncross-linked PPXTA and PPTA. The results for PPTA and PPXTA are compared in view of the difference in their molecular backbone. More importantly, the effect of the formation of intermolecular cross-links in PPXTA is assessed. The obtained properties are critically related to the molecular structure and to the morphology, and compared to the theoretical perfect crystal properties obtained with molecular simulations.

Present address: * Union Carbide Corporation, P.O. Box 670, Bound Brook, NJ 08805 USA.
‡To whom correspondence should be addressed.

0022–2461

The shear modulus is obtained via torsional experiments and the lateral compressive properties are deduced from transverse compression experiments. Because of the small lateral dimensions of high performance fibres ($\approx 10\,\mu m$), the axial, transverse, and torsional properties are the only deformation properties experimentally available. Whereas the axial and torsional properties are routinely measured, the transverse properties pose an experimental challenge. We present here a new technique and machine, available at Oak Ridge National Laboratories (ORNL), that facilitate these measurements.

Both the compressive and tensile behaviour of high performance fibres are influenced by the lateral properties. Oriented fibres yield in compression by the formation of kink bands, thought to be initiated by buckling of interacting chains or fibrils [3, 4], or by a shear instability [5]. Regardless of the specific instability mechanism, it appears that the shear modulus and shear strength are critical to the compressive behaviour. Observation of the intermolecular shearing within kink bands in axially compressed extended-chain polymers led to the design of cross-linkable PPXTA fibres [6, 7]; it is expected that the cross-links restrict intermolecular shearing. The transverse properties are important since a lateral tensile strain develops within kink bands during axial compressive deformation [8]. The importance of shear properties on the tensile behaviour of oriented extended-chain polymers has been illustrated with a recent constitutive model [9]. The tensile properties of the polymer were related to the aspect ratio of the molecules, the interchain shear properties and the chain tensile properties. Other models have shown the dependence of the polymer tensile modulus on the shear modulus [10, 11] and of the tensile strength on the shear strength [12].

An evaluation of the shear and transverse moduli is of fundamental interest regardless of their influence on the tensile and compressive properties, because the ratio of the shear (or transverse) modulus to the tensile modulus is indicative of the materials' anisotropy [13]. Traditionally, because of the difficulty of measuring a transverse modulus on fibres with small diameters, the shear modulus has been used to define the anisotropy ratio.

The production of transverse deformation may be significant during fibre fabric processing, such as pleating or other setting operations [14, 15]. Substantial lateral compressive stresses may be imposed on the fibres in end-use applications, for example in a fabric at the yarn cross-over points [15]. These stresses may lead to fibre damage, thereby preventing effective use of the high longitudinal strength of the fibres. Finally, the transverse properties of fibres may have an influence on the energy-absorbing capacity of high performance fibre composites under transverse loading.

1.1. Lateral compression experiments

A number of methods have been previously used to examine the lateral properties of polymer fibres. Mason [14] tested, in lateral compression, wool fibres and wool fibres that had been cross-linked with formaldehyde. Weights were applied on an assembly that contained four layers of pairs of 50 μm fibres interspaced with 5 mm wide glass bars. The tests were done in water or acid solution, at different temperatures, with loads up to 400 g. A measure of the lateral elasticity at room temperature was given by the load–deformation relation. The wool and formaldehyde-treated wool exhibited the same deformation behaviour, regardless of the solution used. The fibre assembly was then subjected to a loading and unloading cycle at 100 °C, until steady state deformation was reached. The permanent viscous deformation, at the end of the on/off cycles, was highest for the native fibres, and least for the formaldehyde-treated fibres. The permanent deformation of the native fibres was slightly reduced by the use of an acid medium, and was greatly increased when using a lower temperature of 70 °C. Mason pointed out that acid and formaldehyde treatment, or lower temperature, also reduces the effectiveness of pleating operations on wool fabrics. Based on the semi-quantitative agreement of the lateral compression tests and fabric-pleating tests, it was concluded that lateral compression is a possible mechanism of setting process in wool fabrics.

Phoenix and Skelton [15] used an Instron machine fitted with two parallel flat steel platens to test the lateral compressive deformation behaviour of organic polymer (Kevlar, nylon, polyester) and graphite fibres. One to four parallel fibres were mounted in the lower platen, and the upper platen was lowered at a speed of $0.058\,mm\,min^{-1}$ while the load versus displacement was recorded. The organic fibres were reported to exhibit non-linear transverse deformation, substantial plastic flow, and no apparent rupture. In contrast, the load–displacement behaviour of the graphite filaments was elastic up to brittle fracture. Mathematical expressions were given that make it possible to calculate the width of the contact zone $2b$ [16], the transverse elastic modulus E_t, and the maximum shear stress at yield τ_{max}; the yield point was taken as the proportional limit. These expressions are described in Section 3.

Batra and Syed [17] studied the lateral compressive behaviour of nylon and polyethylene terephthalate (PET) fibres by following the change in the contact width $2b$, as a function of the applied force. The test apparatus consisted of an optical microscope and a lever arrangement to apply the load in 200 g increments. The elastic modulus E_t was estimated from the slope of the linear portion of the curves $(2b)^2$ versus the applied load [16] (see Section 3). The non-linearity of the graphs at higher strains was attributed to the plastic and inhomogeneous nature of the deformation. This was confirmed with scanning electron microscopy (SEM) examinations of the tested specimens. Parallel surface striations were observed on the cross-sections of laterally deformed fibres. In some excessively deformed materials, the parallel striations developed kinks lining up along a direction approximately 45° to the plane of compression. Large cracks appeared to nucleate and propagate along the striations. Thus regions in which the deformation was

highly concentrated were observed. It was suggested that the striations were aligned with slip planes along which the inelastic deformation of the filament was the highest.

Jawad and Ward [18] provided a solution for the diametrical compression of a transversely isotropic elastic cylinder between parallel plates under conditions of plane strain, in a manner similar to Phoenix and Skelton [15]. Again the mathematical expressions that make it possible to calculate the contact width $2b$ [16] and the transverse elastic modulus E_t are described in Section 3. The samples studied were isotropic and oriented rods of nylon and linear polyethylene (PE), and had diameters ranging from 2.5 mm to 8.5 mm. Both the contact width and the diametrical compression were measured. For small diameter extrudates, the test specimens were compressed between two blocks of glass and the contact zone was viewed in reflected light. For large diameter samples, a dead loading compression creep apparatus was used. The upper side of the specimen was lightly coated with ink and the contact width was visualized in transmitted light. In both cases, the samples were left unloaded for 5 to 10 min between each increasing load. Good agreement was found for the values of $S_{11} - S_{13}^2/S_{33}$ from contact width and total compression measurements. $S_{11} - S_{13}^2/S_{33}$ represents the transverse compliance S_{11} only if the fibre is very anisotropic in the fibre or 3 direction. The value of the transverse modulus of linear polyethylene $E_t = 1/S_{11}$ was found to decrease with increasing extrusion ratio. This change was small when compared with the change in the longitudinal Young's modulus.

Kawabata [19] developed an instrument that recorded the compression force as a function of fibre diametrical change under a constant rate of loading. In this instrument, a single fibre was compressed between a platen and a punch. The punch was driven through a rod connected to an electromagnetic power drive with a load capacity of 5 kg. The size of the square punch was 0.2 mm in length, which was considered sufficient to ensure plane strain deformation of 10 μm range fibres. The deformation was detected with a linear differential transformer with a resolution of 0.05 μm. Various carbon, ceramic, glass and organic polymer fibres were tested. The transverse modulus was calculated using the mathematical expression for the diametrical compression developed by Jawad and Ward [18]. Kevlar fibres were found to yield and showed hysteresis. The carbon, ceramic and glass fibres did not yield and their compression curves were almost straight up to the point of brittle fracture. The ultimate apparent stresses for the ceramic fibres and carbon fibres were much higher than the apparent yield stress $\bar{\sigma}_y$ for the aramid fibres. The apparent stress was defined as the load divided by the length of the tested fibre (0.2 mm) and its diameter. The criteria for yield was the onset of non-linear transverse deformation. Thus the yield stress $\bar{\sigma}_y$ was assumed to be analogous to the stress at the proportional limit $\bar{\sigma}_p$. It was pointed out that the maximum stress in the cross-section of the fibre is much higher than the apparent stress because of the stress distribution. Correlations between the transverse modulus E_t and the longitudinal modulus E_l were observed. For the brittle-type materials, the value of E_t decreased sharply with increasing E_l. However when the various organic polymer fibres were considered, the value of E_t increased slightly with increasing E_l.

Knoff [20] measured the lateral compression properties of PPTA fibres of different equilibrium water content, using the instrument developed by Kawabata [19]. The transverse modulus E_t and maximum shear stress at yield τ_{max}, called shear strength, were calculated with the mathematical expressions derived by Phoenix and Skelton [15]. The yield point was taken not as the proportional limit but as the point of maximum slope in the pseudo-linear region of the load – displacement curves. Both the modulus and the shear strength were found to decrease with increasing water content. This was attributed to the void content being filled with water, with the water hydrogen-bonded with PPTA molecules and therefore interfering with intermolecular hydrogen bonding, and the crystalline imperfection in fibres not heat treated at high temperature.

Kotani and colleagues [21] reported transverse moduli for various commercial organic fibres, including PET, PE, and a thermotropic liquid-crystalline copolyester of hydroxy benzoic acid-hydroxy naphthoic acid (HBA–HNA) (Vectra) polymer. The apparatus used allowed compression of the fibre specimen between two glass plates. The contact zone at the upper glass plate was viewed with an optical microscope using reflected light, through a hole in the upper loading beam. The diametrical compression was measured using a pair of linear displacement transducers of accuracy 0.1 μm. The specimen length was 5 mm. A special loading and recovery procedure was used to remove time-dependent or viscoelastic effects. PET fibres were the most elastic materials; permanent deformation was not detected so no conditioning was used. In contrast, PE and Vectra showed some plasticity, the recovery was not complete and the conditioning system was used. The elastic transverse modulus was calculated with the expressions derived by Jawad and Ward [18], using the contact width or the diametrical compression. Good agreement was found for the values determined both ways, although the values obtained from the diametrical compression were subject to less error and considered more reliable. Also plasticity could be detected as permanent deformation of the compressed diameter but was not detectable from observations of the contact zones since the contact zone always shrinks back to zero width on removal of the load.

1.2. Torsional experiments

Allen [13] characterized the mechanical anisotropy of PPTA and PBZT (poly(*p*-phenylene benzobisthiazole) fibres. A general consideration of anisotropic fibre behaviour was presented to explore the states of stress for several simple test geometries such as tensile testing, torsion, and pure bending. Fibre torsional modulus and strength were measured using

a torsional pendulum apparatus with pendulum discs having moments of inertia 56 and 115 g mm^2 [13, 22]. The fibre torsional modulus was obtained from measurements of the dynamic oscillations of the torsional pendulum using the equation described in Section 2. The torsional modulus for Kevlar 49 and PBZT were respectively 1.8 and 1.3 GPa, low values compared to their tensile modulus of 130 and 200 GPa. A critical torsional strain was estimated by imposing various amounts of torsional strain on a sample and measuring the elastic or reversible component of the applied twist. The reversible region of behaviour for Kevlar 49 and PBZT existed, respectively, below a 10 and 5% surface strain. At higher strains, Kevlar 49 fibres split longitudinally. The splitting was attributed to permanent slippage between radial planes of hydrogen-bonded PPTA chains or between weakly bonded microfibrils. An apparent shear strength was calculated as the product of the critical torsional strain and torsional shear modulus. This apparent shear strength was therefore 180 and 65 MPa respectively for Kevlar 49 and PBZT, lower than a fibre typical axial strength of 2 to 3 GPa.

Allen [23] provided a theoretical solution of the torsional modulus under a multiple stress state of torsion and axial tension. The torsional modulus was predicted to increase for anisotropic fibres with increasing tensile load. The apparent or measured shear modulus G_m was $G_m = G + A\sigma_z$ where G is the true shear or torsional modulus, A is a measure of the fibre's mechanical anisotropy, and σ_z the applied axial tensile stress. The measured shear modulus G_m was found to increase with axial load for Kevlar 49. However, G_m was constant at all tensile loading for an isotropic glass fibre, as predicted by the equation. These experiments were used to estimate the anisotropy term A. A was highest for Kevlar 49, slightly lower for nylon, and zero for glass.

DeTeresa and co-workers [24] also reported an apparent increase in fibre torsional modulus with axial tensile stress for PPTA and PBZT fibres. A linear relationship between axial compressive strength and torsional modulus was experimentally found on a number of Kevlar, poly(*p*-phenylene benzobisoxazole) PBZO, and PBZT fibres, supporting the concept of compressive failure due to an elastic microbuckling instability. It was emphasized that the weakest shear modulus provided for an estimate of the compressive strength needed. In the case of radially arranged PPTA, the lowest shear modulus is the torsional modulus of shearing between hydrogen-bonded sheets.

Mehta and Kumar [25] reported torsional moduli and damping factors of a number of polymeric fibres (Kevlar, PBZO, PBZT and Vectra) and carbon fibres as a function of a vacuum level and of temperature. The moduli were measured using a free-torsional pendulum placed in a vacuum oven. The moment of inertia of the pendulum was 9.24 g mm^{-2} and the total weight of the pendulum was less than 0.75 g. The damping factor was found to be significantly different for different fibres and proportional to the period of oscillation, suggesting that damping was essentially due to aerodynamic effects. The variation in shear modulus for the different fibres was explained in terms of their molecular structure. The shear modulus of Kevlar 49 was tested at different temperatures and compared to available data on the temperature dependence of Kevlar 49's compressive strength. A linear relationship between the shear modulus and the compressive strength was found, supporting the buckling instability as the operating compressive failure mechanism in Kevlar 49. However the relation between the compressive strength and torsional modulus did not hold for other materials.

1.3. Cross-linkable PPXTA fibres

PPXTA (poly(*p*-1,2-dihydrocyclobutaphenylene terephthalamide)) was developed to modify the macroscopic properties of PPTA (poly(*p*-phenylene terephthalamide)), including its deformation behaviour. PPXTA polymer is synthesized from the XTA monomer instead of the conventional terephthalic acid (TA) used for PPTA [26, 27]. A schematic of PPTA and of PPXTA is displayed in Fig. 1. The benzocyclobutene (BCB) moiety is a thermally activated cross-linking group that reacts by the opening of the cyclobutene ring at temperatures of approximately 350 °C, above the synthesis and spinning temperatures (25 °C, 100 °C) but below the polymer degradation temperature (500 °C). Thus PPXTA may be cross-linked in the solid state during a post-spinning heat treatment, while retaining its orientation and degree of order.

The processing, microstructure, and properties of cross-linkable PPXTA fibres have been described elsewhere [28, 29]. Differential scanning calorimetry experiments indicated that the exothermic cross-linking reaction starts at 300 °C and is completed at about 425 °C. Thus one may compare uncrosslinked materials heat-treated below 300 °C to cross-linked materials heat-treated above 300 °C. Ideally, the material

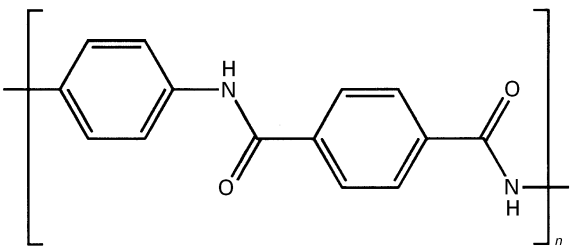

PPTA

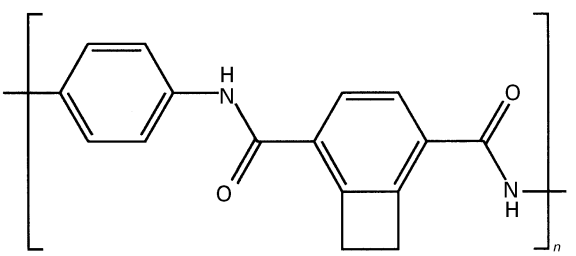

PPXTA

Figure 1 Chemical structure of PPTA and PPXTA.

evolves during heat treatment from an anisotropic array of extended molecules to a more isotropic network of covalent bonds. The higher the heat-treatment temperature and time, the greater the density of intermolecular cross-links. This increase in cross-linking density is coupled with an improvement in orientation and degree of crystallinity.

The morphology of PPXTA is similar to that of PPTA. Lyotropic liquid crystalline polymers such as PPTA and PPXTA are known to form a microfibrillar network during coagulation of the oriented lyotropic solution in a non-solvent bath (water) [30, 31]. The crystalline structure of PPXTA is similar to that of PPTA, with the molecules being hydrogen bonded, the distance between hydrogen-bonded planes being greater in the case of PPXTA ($a = 0.91$ nm) [28] than in the case of PPTA ($a = 0.79$ nm) [32]. The hydrogen-bonded planes are arranged radially for PPTA [33, 34]. The X-ray diffraction patterns of uncross-linked and cross-linked PPXTA fibres appeared similar, suggesting that most of the cross-links preferentially form in the grain boundary phase between crystallites. Furthermore, the cross-linking reaction may be restricted within the microfibrils. The nature of the cross-linking reaction was not firmly established. Solid state ^{13}C nuclear magnetic resonance (NMR) was consistent with the formation of a carbon–carbon double bond in the cross-linked materials [35]. This is in agreement with the suggestions of Marks [36, 37] on the products of BCB homopolymerization. A thermal degradation process was thought to take place concurrent with cross-linking during the heat treatment, and is probably responsible for the observed loss of tensile strength at high temperature [38].

2. Experimental procedures

2.1. Molecular modelling

Molecular modelling was performed to estimate the elastic constants of ideal perfect crystals of PPTA, PPXTA, and PPDXTA, with the CERIUS modelling software and the Dreiding II force field [39]. PPDXTA contains a benzo-di-cyclobutene (BDCB) [40] instead of a benzocyclobutene (BCB) in the diacid moiety, and potentially may contain twice as many cross-links as PPXTA. The default settings of the Dreiding II force field were used except the convergence criteria (r.m.s. force in (kcal mol^{-1})/nm and r.m.s. gradient in (GPa nm^{-1}) were set at 0.05. The Northolt structure of PPTA [32] was built and its energy minimized. For PPXTA, model 1 of the Northolt type [28] was used. The crosslinks that were introduced contained a carbon–carbon double bond because of the available data showing the formation of a carbon-carbon double bond in the cross-linked materials. Four original PPXTA unit cells were used to avoid the creation of cross-linked dimers, and instead to create cross-linked (1–$\bar{1}$0) planes.

2.2. Materials and heat-treatment

As-spun PPXTA fibres synthesized at the University of Michigan and spun at DuPont were heat-treated under 0.3 GPa of tension, in a tube furnace in a nitrogen atmosphere, for 30 to 120 s, at intermediate temperatures (260 °C) to increase crystallinity and orientation and at higher temperatures (above 300 °C) to trigger the cross-linking reaction. The degree of cross-linking varies with the heat treatment conditions [29].

2.3. Torsional experiments

Fibre torsional moduli G were obtained for PPXTA and PPTA (Kevlar 49 and 149) from free vibration torsional experiments. The apparatus and measurements have been described by DeTeresa *et al.* [22]. Single fibres were bonded onto cardboard tabs to produce a 2.54 cm gauge length. The fibre was suspended on a fixed grip inside a vacuum oven. A weight of 10 g was hung to the other tab. The experiment consisted in imposing a 180° twist to the fibre/weight system and allowing the fibre to rotate freely. The moment of inertia I of the weight was calculated from the relation $I = 0.5\,mr^2$ where m is the mass of the weight and r is the radius. I was 153 g mm^{-2}. A toothpick was mounted on the bottom of the weight for easier timing of the period of oscillation. The oven was closed and a vacuum was activated to limit the damping effect observed upon experiments in air. Once the fibre was perfectly still, the release knob was opened and closed to allow a wind current to start the oscillation of the system initiated by a 180° twist of the fibre, as suggested by Mehta and Kumar [25]. No lateral motions of the pendulum were observed. While the fibre was oscillating, the half period was measured several times with a stopwatch. For each fibre type, the measurements were made on four samples. Because of the slight damping, the first four half periods were measured for each sample to ensure comparability of the data. The average value of these measured periods was used to determine the torsional modulus G, using the equation

$$G = 8\pi IL/T^2 r^4 \quad (1)$$

where I, L, T, r are respectively the moment of inertia of the torsion pendulum (153 g mm^{-2}), the fibre sample length (2.54 cm), the oscillation period, and the fibre radius (typically 7.8 to 10 μm). Three diameters of each fibre sample were measured with optical microscopy using video camera and NIH Image 1.54 imaging software on a Macintosh.

2.4. Transverse compression experiments

Lateral compression experiments were performed on PPXTA fibres, SiC Nicalon (NL-200) fibres, Al_2O_3 FP fibres, PET Dacron (lot #840-140-R02-68) fibre, and the polyamides nylon 6,6 (lot #840-140-R20-717), Nomex (lot #200-100-R79-430), and Kevlar 29, 49, and 149 fibres. Nomex is the tradename for poly(*m*-phenylene isophthalamide) (MPDI). The first idea to evaluate transverse compression properties was to use a nanoindenter and obtain an elastic modulus and hardness. The obtained modulus and hardness would be local and, because of the conical geometry of the indenter, would have to be deducted from the complex

method outlined by Oliver and Pharr [41]. Exactly what the measured elastic modulus would represent is uncertain. One could substitute the conical indenter with a flat indenter; in this case the available method to estimate a value for the transverse modulus, outlined by Phoenix and Skelton [15] and Jawad and Ward [18], requires that the flat indenter be much larger than the fibre to ensure plane strain conditions. The precision of the nanoindenter becomes inappropriate, and furthermore the load estimated to be necessary for fibre yield is not available with the nanoindenter. Thus the interfacial test system (ITS) machine built at Oak Ridge National Laboratories was used. The ITS machine was designed to measure the interfacial properties of composites by means of single-fibre indentation tests, and is described elsewhere [42, 43].

The ITS machine consists of an optical microscope, a system of microstep-positioned xyz translation stages with 1 μm repeatability on the xy plane and 0.1 μm repeatability in the z direction, and an indentation table. The flat-ended punch is stationary and the moving table supporting the sample is translated up in the z direction towards the punch. The displacements in the z direction are determined using a capacitance gauge with 5 nm resolution. The accuracy of the displacement is 1-step calibrated as (1/97.93) μm/steps. The load was measured with a 1000 g load cell. The difficulty of this experiment arises from the small size of the fibre which requires that both the flat-ended punch and the substrate on the moving table have a roughness much smaller than 10 μm, and, more challenging, that the flat-ended punch be exactly parallel to the substrate. To ensure low roughness for the punch and the substrate, pieces of glass slide of roughness less than 0.01 μm were used for both. A glass slide was glued to the moving table with a thin layer of wax to provide for the substrate. A cylindrical glass disc of diameter 2 mm was cut out of a slide with an ultrasonic device, to provide for the flat end of the punch. Fig. 2 displays a schematic of the punch, outlining the method used to precisely orient the punch parallel to the substrate. The glass disc was glued to an aligning sphere, itself glued to a connector attached to the stationary load cell. The two component Epoxy Epon 828 glue (manufactured by Shell) was allowed to harden overnight while the glass punch was in contact with the glass substrate with no fibre between, as done by Cunniff [44]. In order to account for the compliance of the epoxy glue, the machine compliance, typically 1.5 steps/g in raw data, was taken into account.

For each experiment, the table supporting the fibre was displaced towards the flat-ended indenter at a speed of 20 steps/s or 91.8 nm s^{-1} (0.0918 μm s^{-1}), while the load was continuously recorded up to 1000 g. A load–displacement curve was recorded. No load and unloading conditioning cycle was performed prior to the test. Mason [14] and Kotani, Sweeney, and Ward [21] performed a conditioning step before testing; Kawabata [19] and Phoenix and Skelton [15] did not. The flattened fibre was observed with the ITS optical microscope to ensure that the contact between the flat-ended punch and the fibre sample had been uniform. Some of the flattened fibres were subsequently observed with an Optiphot2-POL Nikon optical microscope. The width of the flattened fibre $d_\perp$ was measured and compared to the original diameter d. Between each alignment the compliance of the machine was measured. The length of the flattened fibre l, approximately equal to the diameter of the glass punch or 2 mm, was measured on each sample using a Nikon profile projector. The diameter $d = 2R$ of the fibres was measured as indicated in the torsional experiments section.

2.5. Transverse compression experiments with the "pipette test"

Lateral compression tests were also performed by compressing a single fibre between a glass pipette of diameter 7.25 mm and a glass slide with a weight on top of the pipette, see Fig. 3. This test does not require special equipment and has been described by Jiang *et al.* [29]. The deformed fibre was observed with an Optiphot2-POL Nikon optical microscope. The diameter d_p of the widest area of the deformed fibre was compared to the diameter of the original fibre d, and an apparent plastic strain $\bar{\xi}_p = (d_p - d)/d$ was calculated. A weight greater than 100 g lead to fibrillation and cracking of the cross-linked fibres, and therefore to an apparently very deformed fibre. Thus the test was done with a load of 100 g, and all the diameters were measured on uniformly deformed fibres.

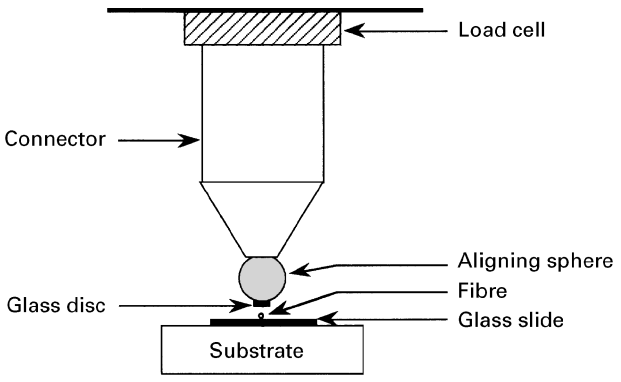

Figure 2 Schematic of the punch used in the lateral compression experiments.

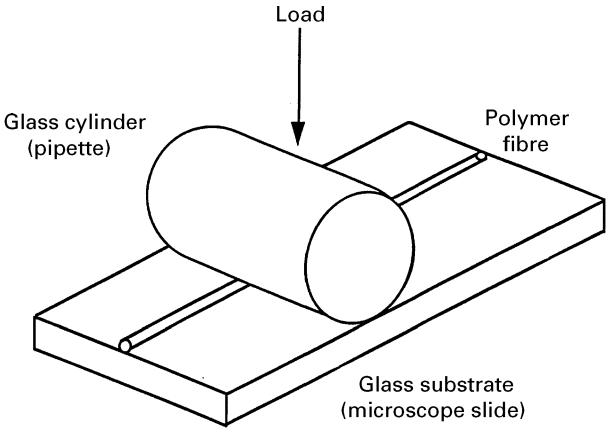

Figure 3 Schematic of the "pipette test" (from [29]).

2.6. X-ray diffraction of heavily laterally deformed PPXTA

Wide angle X-ray diffraction (WAXD) patterns were obtained on PPXTA fibres, heavily laterally deformed between a glass pipette and a glass slide, or undeformed. The PPXTA fibres used for these experiments were spun at the University of Michigan; the processing has been described by Jiang *et al.* [29]. The diffraction patterns were performed at Wright Patterson Air Force Base on flat-film cameras with pinhole collimation. The X-ray source was CuK_α radiation from a Rigaku RU-300 or RU-200 rotating anode generator with a graphite crystal as the monochromator. The fibres were attached vertically onto the exit of the collimator. The camera length was typically 3 cm.

3. Calculation of transverse properties

Upon transverse compression of the fibres, the ITS machine recorded the compression load as a function of fibre diametrical change or lateral displacement in the loading direction. The raw data was a load P in g versus a global displacement in steps. The fibre displacement u in steps was calculated by removing from the global displacement the displacement of the machine (compliance of the machine in steps/g times load P in g). From P and u, an apparent stress $\bar{\sigma}$ and apparent relative strain $\bar{\xi}$ were calculated using the following equations

$$\bar{\sigma}(Pa) = \frac{9.81P(\mathrm{g})}{l(\mathrm{mm})d(\mu\mathrm{m})}10^6$$

and

$$\bar{\xi} = \frac{u(\mathrm{steps})}{97.3\,\dfrac{\mathrm{steps}}{\mu\mathrm{m}}\,d(\mu\mathrm{m})} \qquad (2)$$

The relative strain $\bar{\xi}$ is the sum of the absolute strain $\bar{\xi}_o$ which is zero at zero stress and of an offset term $\Delta\bar{\xi}$. Here all the results are expressed in terms of the apparent stress and apparent relative or absolute strain.

Phoenix and Skelton [15] and Jawad and Ward [18] presented a theoretical discussion of the transverse compression behaviour of a linear elastic homogeneous transversally isotropic cylinder, with the transverse axis defined as "1" and the longitudinal axis defined as "3". Using their theoretical results and the experimental transverse stress $\bar{\sigma}$–strain $\bar{\xi}$ behaviour, it is possible to determine the transverse elastic modulus $E_t = 1/S_{11}$. Using Phoenix and Skelton's analysis, one may calculate a maximum shear stress τ_{max} in the fibre transverse plane at which the fibre yields, when $\bar{\sigma}$ reaches the yield stress $\bar{\sigma}_y$. τ_{max} is also called the transverse shear strength. Both sets of authors assumed that yielding takes place when the transverse stress–strain behaviour deviates from pseudo-linearity. A more accurate definition of τ_{max} is the shear stress in the fibre transverse plane when $\bar{\sigma}$ reaches the stress at the proportional limit $\bar{\sigma}_p$. The geometry of the setup is shown on Fig. 4. The problem treated is one of plane strain with no displacement developing

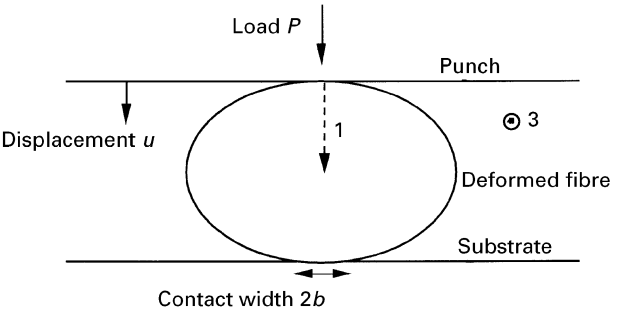

Figure 4 Transverse compression of a transversely isotropic fibre.

along the fibre axis direction. Only small displacements are considered. The material is assumed to have a linear elastic behaviour. The fibre is assumed to be strongly anisotropic in the "3" direction. The calculations assume that the contact width $2b$ is smaller than the diameter of the fibre d.

To calculate the transverse modulus we use the expression for the strain derived by Jawad and Ward [18] which was subsequently used by Kawabata [19] and Kotani and colleagues [21]. Using our notation, this equation is

$$\bar{\xi}_o = \frac{1}{2}\left(\frac{b}{R}\right)^2\left[0.19 + \sinh^{-1}\left(\frac{R}{b}\right)\right] \qquad (3)$$

where b is the half width of the contact zone, which may be calculated instead of measured experimentally. The mathematical expression for b given by Hadley *et al.* [16] is

$$b = R\left[\frac{8\bar{\sigma}(S_{11} - S_{13}^2/S_{33})}{\pi}\right]^{1/2} \qquad (4)$$

which becomes $b = R\,(8\bar{\sigma}S_{11}/\pi)^{1/2}$ with the anisotropy assumption that $S_{11} \gg S_{13}^2/S_{33}$. Thus the expression for the strain is

$$\bar{\xi}_o = \frac{4\bar{\sigma}S_{11}}{\pi}\left\{0.19 + \sinh^{-1}\left[\left(\frac{8\bar{\sigma}S_{11}}{\pi}\right)^{-1/2}\right]\right\}$$
$$= f(\bar{\sigma}, S_{11}) \qquad (5)$$

Knoff [20] used the expression derived by Phoenix and Skelton which differs from the Jawad and Ward expression only in that 0.19 is replaced by -0.5, and 8 is replaced by 2. Using the two slightly differing equations, Knoff [20] and Kawabata [19] obtained similar results on PPTA.

Our standard method to calculate the transverse elastic modulus $E_t = 1/S_{11}$ is described here. The exact equation $\bar{\xi}_o = f(\bar{\sigma}, S_{11})$ or $\bar{\xi} = f(\bar{\sigma}, S_{11}) + \Delta\bar{\xi}$ was fitted to the experimental apparent stress–strain curve $\bar{\sigma}(\bar{\xi})$, the two fitting parameters being S_{11} and $\Delta\bar{\xi}$. Thus the fitting procedure was used to solve the problem of the uncertainty in the strain at zero stress or in the offset term $\Delta\bar{\xi}$. The fitting procedure was done with the software Kaleidagraph, necessitating calculations of the derivatives of $\bar{\xi}$ with respect to the two fitting parameters. Fig. 5 shows $\bar{\sigma}(\bar{\xi})$ and the smoothed derivative $d\bar{\sigma}/d\bar{\xi}(\bar{\xi})$ for a sample of PPXTA heat-treated at 260 °C for 30 s under tension. The proportional limit on the $\bar{\sigma}(\bar{\xi})$ curves was taken as the

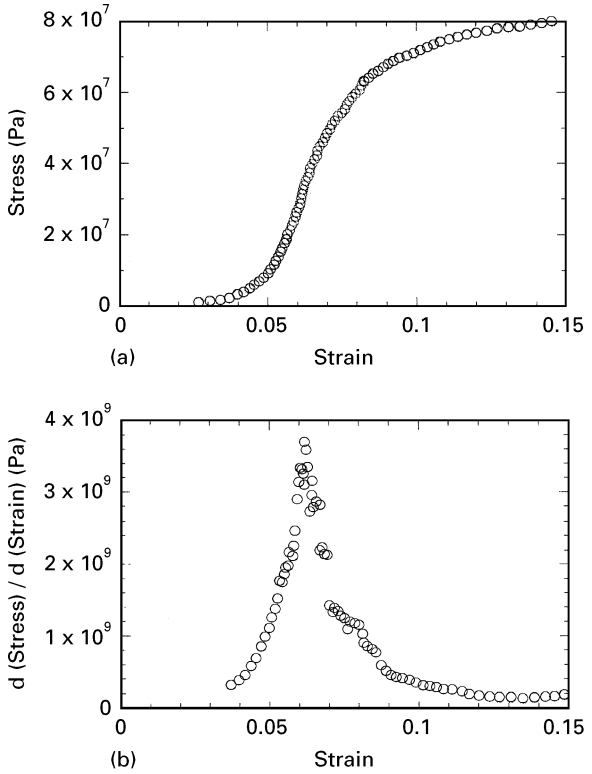

Figure 5 Plots of (a) $\bar{\sigma}(\bar{\xi})$ and (b) $d\bar{\sigma}/d\bar{\xi}(\bar{\xi})$ for PPXTA heat-treated at 260 °C for 30 s under tension. The derivative was smoothed over nine data points.

point of maximum derivative. The stress at the proportional limit was termed $\bar{\sigma}_p$. A total of 21 data points centered on the proportional limit were used for the fitting procedure, corresponding to a range of displacement of 20 times (1/97.93) μm or 0.205 μm. The curves $d\bar{\sigma}/d\bar{\xi}(\bar{\xi})$ did not always present an obvious single maximum, and sometimes the maximum of the middle peak of three peaks or the minimum between two peaks was used. The stress–strain curves $\bar{\sigma}(\bar{\xi}_o)$ and their fitting curve $\bar{\xi}_o = f(\bar{\sigma}, S_{11})$, respectively, obtained using the calculated values of $\Delta\bar{\xi}$ and of S_{11}, are presented in Fig. 6 for PPXTA as-spun and heat-treated at 260 °C for 30 s under tension. A good agreement between the experimental and calculated curves is seen in the pseudo-linear region of the curves.

The transverse shear strength τ_{max} may be calculated using the equations derived by Phoenix and Skelton [15], and the determined values of $\bar{\sigma}_p$ and S_{11}. Phoenix and Skelton's original equations are given as a function of the yield stress $\bar{\sigma}_y$ instead of the stress at the proportional limit $\bar{\sigma}_p$, because of the assumption of equivalence between yield point and proportional limit. The solution gives

$$\tau_{max} = g_m(\bar{\sigma}_p)\left(\frac{\bar{\sigma}_p}{\pi S_{11}}\right)^{1/2} \quad (6)$$

with

$$g_m(\sigma_p) = \max\left\{g(z) + g\left[z\left(\frac{\pi}{\sigma_p S_{11}}\right)^{1/2}\right]\right\} \quad 0 \leqslant z \leqslant \left(\frac{\pi}{\sigma_p S_{11}}\right)^{1/2}\Bigg\} \quad (7)$$

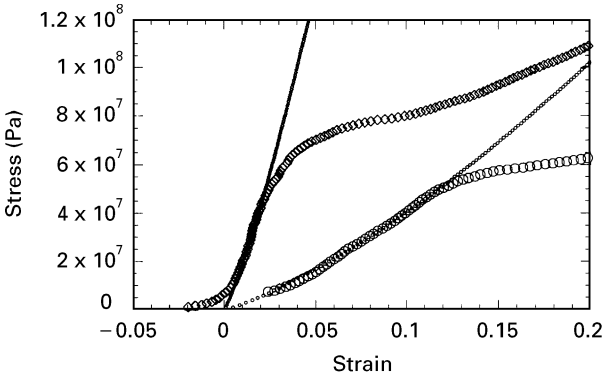

Figure 6 Plots $\bar{\sigma}(\bar{\xi}_o)$ and their fitting curve $\bar{\xi}_o = f(\bar{\sigma}, S_{11})$ for PPXTA before (as-spun, ○) and after heat treatment (◇) at 260 °C for 30 s under tension.

and

$$g(z) = z\left(1 - \frac{z}{\sqrt{1+z^2}}\right) \quad (8)$$

An apparent elastic energy density W, which corresponds to the area under the stress–strain curve $\bar{\sigma}(\bar{\xi})$ up to the proportional limit, as previously defined, may be calculated from the curve fit $\bar{\xi}_o = f(\bar{\sigma}, S_{11})$ and the stress at the proportional limit $\bar{\sigma}_p$. This energy density is given by the equation

$$W = \int_0^{\bar{\xi}_o(\bar{\sigma}_p)} \bar{\sigma} d\bar{\xi}_o = \bar{\sigma}_p \bar{\xi}_o(\bar{\sigma}_p) - \int_0^{\bar{\sigma}_p} \bar{\xi}_o d\bar{\sigma} \quad (9)$$

or

$$W = \frac{1}{2} A\bar{\sigma}_p^2\left[\sinh^{-1}\left(\frac{1}{2A\bar{\sigma}_p}\right) + 0.19\right] + \frac{(2A\bar{\sigma}_p + 1)^{1/2}}{12A}(1 - A\bar{\sigma}_p) - \frac{1}{12A} \quad (10)$$

with $A = 4S_{11}/\pi$.

Assuming that yielding takes place at the proportional limit when $\bar{\sigma}$ reaches $\bar{\sigma}_p$, W corresponds to the energy density stored during elastic deformation, up to yielding.

4. Results and discussion

Structural evidence suggests that PPTA fibres are composed of radially arranged hydrogen bonded planes [33, 34], and therefore possess the symmetry of cylindrical orthotropy. Because of the similarity of PPTA and PPXTA and because PPXTA was spun at Dupont, it is reasonable to assume that PPXTA fibres also possess cylindrical orthotropy. In this case the mutually orthogonal hoop, radial, and axial directions (r, θ, and z) are related to the Van der Waals bonding, hydrogen bonding, and covalent bonding. The compliance matrix for a cylindrically orthotropic material involves nine independent constants. In terms of

engineering constants the matrix may be expressed as follows

$$S_{ij} =$$

$$\begin{pmatrix} 1/E_\theta & -\nu_{z\theta}/E_r & -\nu_{z\theta}/E_z & 0 & 0 & 0 \\ -\nu_{\theta r}/E_\theta & 1/E_r & -\nu_{zr}/E_z & 0 & 0 & 0 \\ -\nu_{\theta z}/E_\theta & -\nu_{rz}/E_z & 1/E_z & 0 & 0 & 0 \\ 0 & 0 & 0 & 1/G_{rz} & 0 & 0 \\ 0 & 0 & 0 & 0 & 1/G_{\theta z} & 0 \\ 0 & 0 & 0 & 0 & 0 & 1/G_{\theta r} \end{pmatrix}$$

where E_i, G_{ij}, and ν_{ij} are respectively the principal Young's moduli, the shear moduli, and Poisson's coefficients. The compliance matrix is reduced to five terms for a transversely isotropic material for which the hoop and radial directions r and θ are equivalent. If PPXTA fibres have cylindrical orthotropy, the torsional modulus G corresponds to the weakest longitudinal shear modulus which involves shear between hydrogen-bonded planes, or to $G_{\theta z}$ [13, 24]. The transverse elastic compression involves compression as well as tension in the radial direction, thus the transverse modulus E_t may be representative of E_θ, or of both E_r and E_θ.

The Young's and shear moduli obtained with molecular simulations on a perfect single crystal of PPTA, PPXTA, and PPDXTA are displayed in Table I. For perfect crystals, the formation of crosslinks almost doubles the value of $G_{\theta z}$ in PPXTA, from 2.0 to 3.8 GPa, and more than doubles the value of $G_{\theta z}$ in PPDXTA. It is also found that $G_{\theta z}$ is higher for uncross-linked PPXTA than for PPTA (2.01 GPa versus 0.8 GPa) and even higher in uncross-linked PPDXTA; this is most likely due to the bulkiness of the cyclobutene group which raises the energy of shifting between adjacent molecules. It is interesting to note that modifying the polymer backbone of PPTA by adding BCB units increases $G_{\theta z}$ by a greater percentage than forming cross-links in PPXTA. Similarly, crosslinking PPXTA increases E_θ by a factor of 1.6 and cross-linking PPDXTA increases E_θ by a factor of 6. Thus the density of crosslinks appears to be critical for the value of E_θ. Adding the BCB and BDCB units to the backbone of PPTA only slightly decreases E_θ, showing that the hydrogen bonds are not much weakened in PPXTA and PPDXTA compared to PPTA.

The results of the torsional experiments are shown in Fig. 7. The experimental values for the torsional modulus G of Kevlar fibres are slightly higher than

TABLE I Young's and shear moduli predicted by molecular simulations for ideal crystals of PPTA and uncross-linked and cross-linked PPXTA and PPDXTA

Moduli (GPa)	E_z	E_r	E_θ	G_{rz}	$G_{\theta z}$	$G_{\theta r}$
PPTA	332.0	71.1	13.8	13.4	0.8	6.3
Uncross-linked PPXTA	259.9	58.5	11.1	9.0	2.0	7.0
Cross-linked PPXTA	154.8	38.7	17.4	6.2	3.8	0.8
Uncross-linked PPDXTA	227.5	52.2	10.7	8.1	3.5	7.0
Cross-linked PPDXTA	164.2	51.8	63.5	8.1	9.0	2.3

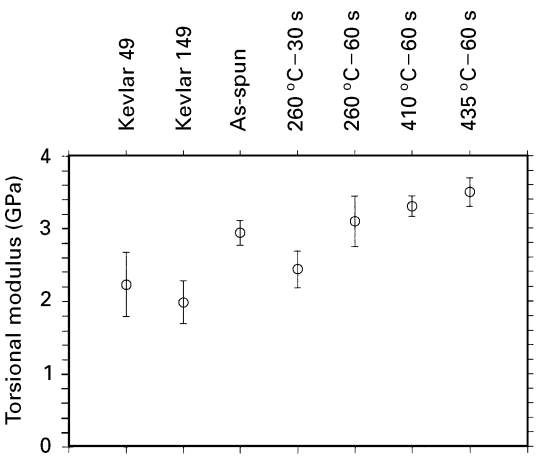

Figure 7 Plots of the torsional modulus G for Kevlar 49 and 149, and PPXTA fibres as-spun and heat-treated under tension at 260, 410 and 435 °C.

previously published values: 1.8 GPa for Kevlar 49 [13] and 1.2 GPa for Kevlar 149 [45]. The observed difference may be related to the stress dependence of the modulus, as discussed by Allen [23]. Nevertheless all the values in this study are comparable since they were obtained using the same experimental conditions. Within the limits of our error, it seems that the torsional modulus of Kevlar 49 is higher than that of Kevlar 149. This would be explained by the higher orientation and lower degree of molecular entanglement in Kevlar 149, which possesses better structural order than Kevlar 49. PPXTA fibres exhibit better torsional properties than Kevlar or PPTA fibres, as predicted by the molecular simulations.

Both the as-spun PPXTA and the PPXTA heat-treated at 260 °C for 1 min are not cross-linked and have similar torsional moduli around 3 GPa. We would expect the fibres heat-treated at 410 °C and 435 °C to display a higher torsional modulus G because of the cross-linking that took place during heat treatment. G only slightly increases from 3.1 GPa for the uncross-linked fibres heat-treated at 260 °C for 1 min to 3.5 GPa for the cross-linked fibres heat-treated at 435 °C for 1 min. Note that the torsional modulus of PPXTA is lowest for fibres heat-treated at 260 °C for 30 s. One explanation of this result could be that the molecules reorient themselves upon a 30 s heat treatment resulting in easier intermolecular shearing and a lower torsional modulus. Upon a 1 min heat treatment, the molecules rearrange themselves to form crystallites. The corresponding increase in intermolecular interaction produces a higher torsional modulus. Interpreting this result in terms of separate orientation and crystallinity improvement should be taken with caution. Because the formation of cross-links during heat-treatment is coupled with the improvement in orientation and crystallinity, the cross-link density and the orientation/crystallinity are interdependent variables. Therefore, it is hard to separate the effects of these two mechanisms.

Fig. 8 shows various plots of $\bar{\sigma}(\bar{\xi})$ obtained from the transverse compression experiments for the SiC Nicalon, Al_2O_3 FP, PET Dacron, and polyamide nylon, Nomex and Kevlar fibres. The limit of the $\bar{\sigma}(\bar{\xi})$

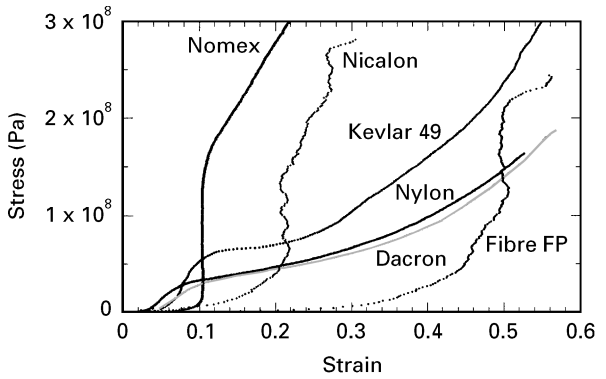

Figure 8 Plot $\bar{\sigma}(\bar{\xi}_o)$ for a SiC Nicalon (lot #NL-200) fibre, an Al_2O_3 FP fibre, a PET Dacron (lot #840-140-R02-68) fibre, and the polyamides nylon (lot #840-140-R20-717), Nomex (lot #200-100-R79-430) and Kevlar 49 fibres.

curves was determined by the load capacity (1000 g) of the equipment. The organic fibres clearly display a non-linear deformation behaviour in transverse compression. The carbon Nicalon and alumina FP fibres did not yield in this experiment, and their compression curves could be considered as almost straight. The noise in the data prevented a modulus from being calculated but it is clear that the modulus for these ceramic fibres is considerably higher than for the organic fibres. It is also likely that these fibres exhibit a brittle failure mode [19], whereas the organic fibres display ductile behaviour. Thus, while ceramic fibres may provide for stiffness, the ductile response of the organic fibres might be an advantage in applications where energy absorbing properties are important.

Comparison of the plots of $\bar{\sigma}(\bar{\xi})$ for the organic fibres shows that the nylon and Dacron fibres are the softest and yield at the lowest stress, Kevlar 49 is intermediate, and Nomex is the hardest of the organic fibres and yields at the highest stress (Fig. 8). We assume that the deviation of $\bar{\sigma}(\bar{\xi})$ from pseudo-linearity is a sign of yielding. The striking difference in behaviour may be explained by the strength and symmetry of the intermolecular bonding. The molecules in Dacron are only weakly bonded by secondary Van der Waals bonds, and the density of hydrogen bonds in nylon is low. In contrast, hydrogen bonds exist in both Kevlar and Nomex. In Kevlar the hydrogen bonds all lie within crystallographic (2 0 0) planes, whereas the hydrogen bonds in Nomex form a three-dimensional network, perhaps explaining Nomex's higher resistance to lateral compression. Nomex's lateral deformation behaviour approaches that of ceramic fibres. Thus, a two-dimensional network of relatively strong intermolecular hydrogen bonds may reduce lateral compressive elastic deformation and delay the shear that takes place [15] at yielding.

These results suggest that highly disordered PPTA, where a large percentage of amide groups would not belong to the crystals, might possess better transverse properties. The assumption is that amide groups in an oriented non-crystalline phase would form hydrogen bonds in all transverse directions. On the other hand, Schadt *et al.* [46, 47] concluded that the molecular segments on the PPTA crystallite surface were not capable of forming hydrogen bonds, based on NMR experiments where the dynamic structure of the terephthalamide and phenylene diamine rings was studied. In addition no major trend was observed for the transverse deformation behaviour of the Kevlar series (Kevlar 29, 49 and 149). It would be interesting to test the transverse deformation behaviour of PPTA-*co*-DXTA, and MPDI-*co*-XXTA [40]. XXTA represents the XTA, DXTA, BXTA and QXTA monomers containing increasing numbers of cross-linkable cyclobutene rings.

The surfaces of transversally compressed fibre samples were observed with optical microscopy. Whereas the nylon, Nomex, Kevlar, and Dacron fibres were seen to be uniformly flattened, no flattening was seen in the fibres FP and Nicalon confirming that these ceramic fibres did not yield. The as-spun PPXTA fibres and fibres heat-treated at 260 °C were uniformly deformed, whereas the fibres heat-treated and cross-linked at 410 °C for 1 and 2 min were often longitudinally split (Fig. 9). The fibres heat-treated at 440 °C for 2 min were often broken perpendicularly to the fibre axis, revealing a brittle fracture mode as a result of intermolecular cross-links or chain ends resulting from the degradation process. In addition, the deformation zone of these highly cross-linked fibres was almost not detectable suggesting that these cross-linked fibres did not remain permanently deformed.

The values of the transverse modulus E_t, stress at the proportional limit $\bar{\sigma}_p$, and shear strength τ_{max} obtained in the present study as well as given by various authors are compared in Table II for PPTA fibres. Kawabata using his machine [19], Phoenix and Skelton using an Instron machine [15], and Knoff using Kawabata's machine [20] find similar, perhaps slightly smaller modulus values. For Kevlar 49, our average value for E_t is 3.5 GPa whereas Kawabata and Phoenix' values are respectively 2.5 and 0.8 GPa. The method used to fit the exact equation $\bar{\xi}_o = f(\bar{\sigma}, S_{11})$, defined in Section 3, was not clearly defined by other authors. The values for the stress at the proportional limit $\bar{\sigma}_p$ found by Kawabata for the Kevlar fibres (and named stress at yield) are approximately twice the values found in this study because of our differing definition of $\bar{\sigma}_p$. Our criteria for the proportional limit is that of maximum slope in the stress–strain curve for accurate determination, whereas Kawabata's criteria was the stress–strain curve departing from a straight line. Given the large standard deviations found in this study, it is not possible to differentiate other aspects of the lateral compressive behaviour of Kevlar 29, 49 and 149. Very little difference was found by Kawabata or Phoenix and Skelton in the behaviour of the various Kevlars. It might be expected that the increased crystalline perfection in these fibres, as revealed by X-ray diffraction, would be associated with better and more uniform intermolecular bonding and, therefore, an increased resistence to transverse compression. However, as mentioned earlier, smaller crystallites may favour the formation of hydrogen bonds in all transverse directions as opposed to being confined in (2 0 0) planes.

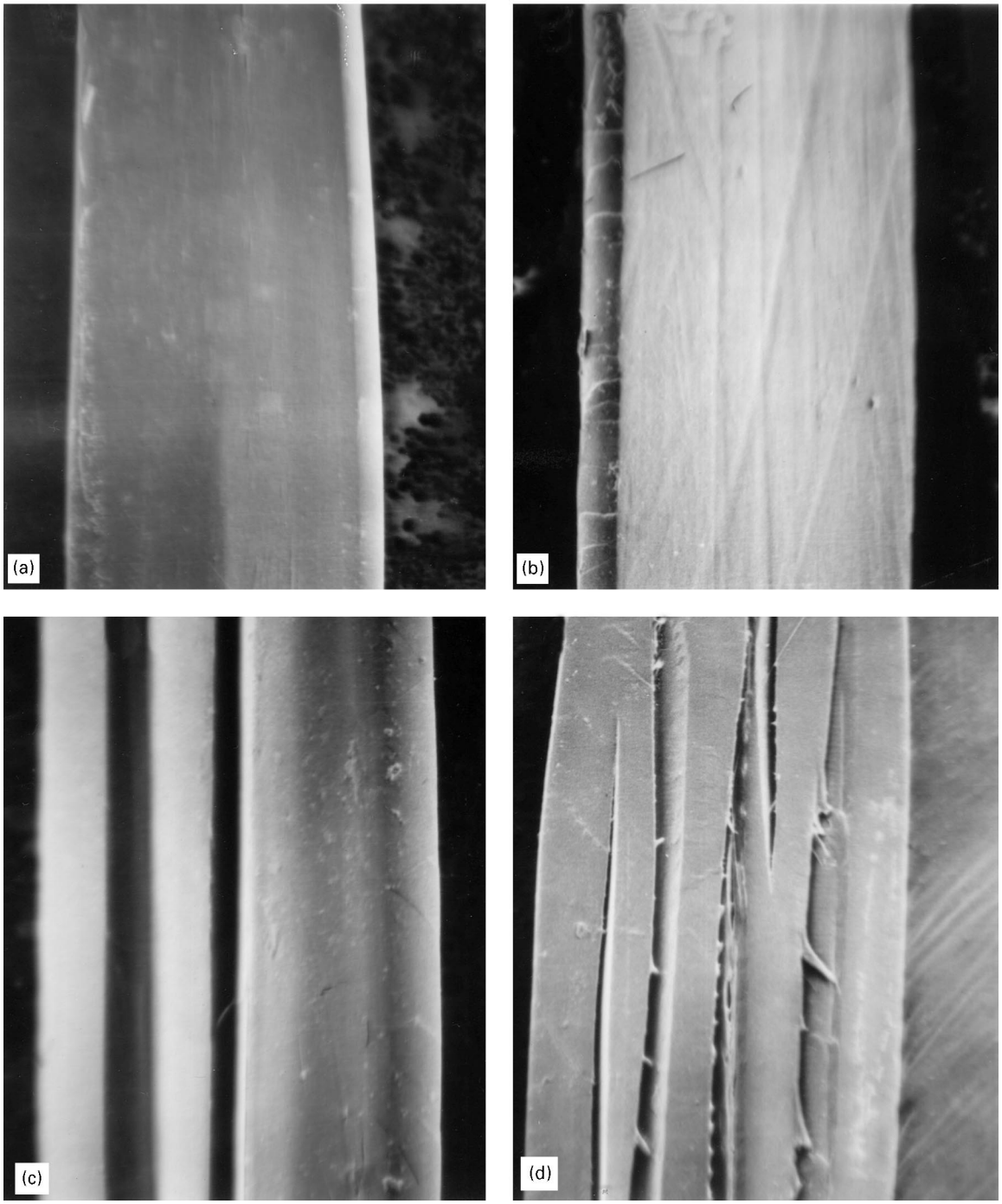

Figure 9 SEM images of laterally deformed PPXTA, (a) as-spun, (b) heat-treated under tension at 360 °C for 30 s, (c), (d) heat-treated under tension at 410 °C for 60 s.

The various properties obtained from lateral compression of commercial organic and ceramic fibres and for the PPXTA fibres are shown in Tables III and IV. Table III lists the number of samples tested for each material, the average values of the transverse modulus $E_t = 1/S_{11}$, transverse stress at the proportional limit $\bar{\sigma}_p$, transverse shear strength τ_{max}, and apparent elastic energy density W (elastic energy density stored up to the proportional limit). The modulus is indicative of the ease of elastic deformation and the proportional limit stress and shear strength are indicative of the onset of local plastic deformation. It is interesting to note that the value of τ_{max} is higher than the value of $\bar{\sigma}_p$. The apparent energy density is related to the elastic energy stored during transverse deformation up to local yielding when the deformation deviates from pseudo-linearity. Table IV lists the values of strains $\bar{\xi}_o$ corresponding to stresses of 100, 200 and 300 MPa. These strains make it possible for us to evaluate the ease of elastic and plastic deformation.

The variation of E_t, $\bar{\sigma}_p$, τ_{max}, W and $\bar{\xi}_o$ corresponding to stresses of 100, 200 and 300 MPa as a function of the fibre are shown in Figs 10–14. The small number of samples, at most four per fibre, the heterogeneity of the samples for the same fibre type, the errors of measurement of the length and diameter of the samples, and the slight misalignment of the punch, all may contribute to the scatter in the results. The nylon fibre

TABLE II E_t, $\bar{\sigma}_p$ and τ_{max} for Kevlar fibres and for experimental PPTA, obtained in the present study and given by Kawabata [19], Phoenix and Skelton [15] and Knoff [20]

		Kevlar 29	Kevlar 49	Kevlar 149	PPTA
E_t (GPa)	Present study	2.5	3.5	2.8	
	Kawabata	2.59	2.49	2.47	
	Phoenix	0.77	0.76		
	Knoff				2.2
$\bar{\sigma}_p$ (MPa)	Present study	25.96	29.8	36.5	
	Kawabata	56	60	77	
τ_{max} (MPa)	Present study	50.5	60.1	63.2	
	Phoenix	46	45		
	Knoff				68

TABLE III Average E_t, $\bar{\sigma}_p$, τ_{max} and W for commercial fibres and PPXTA fibres. "#" represents the number of specimens tested

Material	#	E_t (GPa)	$\bar{\sigma}_p$ (MPa)	τ_{max} (MPa)	W (MPa)
Nylon	2	2.2	13.1	31.5	0.14
Dacron	2	1.6	14.7	29.6	0.22
Kevlar 29	4	2.5	26.0	50.2	0.41
Kevlar 49	2	3.5	29.8	60.1	0.49
Kevlar 149	4	2.9	36.5	63.2	0.74
PPXTA as-spun	3	1.4	27.1	39.4	0.80
PPXTA 260 °C–30 s	3	5.3	34.9	79.7	0.44
PPXTA 260 °C–60 s	4	4.8	29.9	70.4	0.35
PPXTA 260 °C–120 s	4	3.0	38.2	66.4	0.75
PPXTA 410 °C–30 s	4	4.2	35.4	73.0	0.52
PPXTA 410 °C–60 s	4	4.5	44.1	85.4	0.72
PPXTA 410 °C–120 s	4	3.5	48.6	81.4	1.04
PPXTA 440 °C–30 s	2	3.5	52.1	84.7	1.18
PPXTA 440 °C–120 s	3	2.7	46.2	70.6	1.19
Fibre FP	2		141.0		
Nicalon	2		142.0		
Nomex	2		68.9		

TABLE IV Average $\bar{\xi}_o$ at stresses of 100, 200 and 300 MPa for commercial fibres and PPXTA fibres

Material	Strain at 100 MPa	Strain at 200 MPa	Strain at 300 MPa
Nylon	0.377		
Dacron	0.399		
Kevlar 29	0.268	0.448	0.534
Kevlar 49	0.229	0.363	0.428
Kevlar 149	0.247	0.398	0.464
PPXTA as-spun	0.319	0.474	0.556
PPXTA 260 °C–30 s	0.183	0.340	0.426
PPXTA 260 °C–60 s	0.192	0.359	0.447
PPXTA 260 °C–120 s	0.192	0.364	0.455
PPXTA 410 °C–30 s	0.144	0.326	0.408
PPXTA 410 °C–60 s	0.137	0.311	0.373
PPXTA 410 °C–120 s	0.112	0.295	0.365
PPXTA 440 °C–30 s	0.104	0.323	0.421
PPXTA 440 °C–120 s	0.130	0.276	0.352

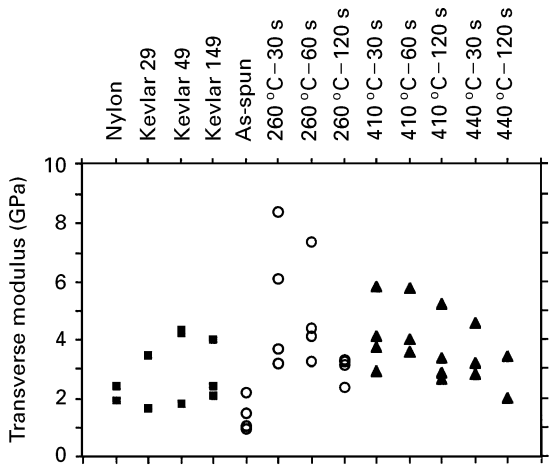

Figure 10 Plot of E_t for various commercial fibres and for PPXTA fibres as-spun and heat-treated under tension at 260, 410 and 440 °C.

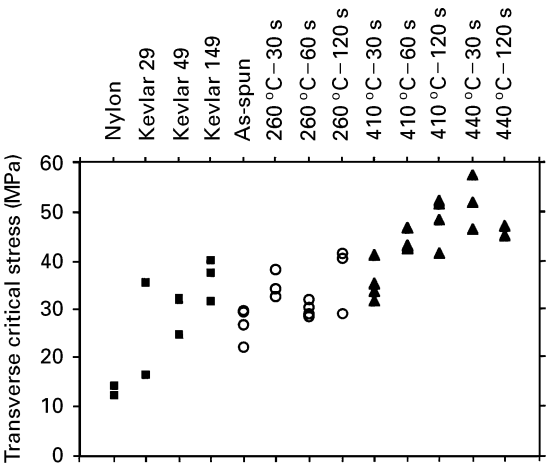

Figure 11 Plot of $\bar{\sigma}_p$ for various commercial fibres and for PPXTA fibres as-spun and heat-treated under tension at 260, 410 and 440 °C.

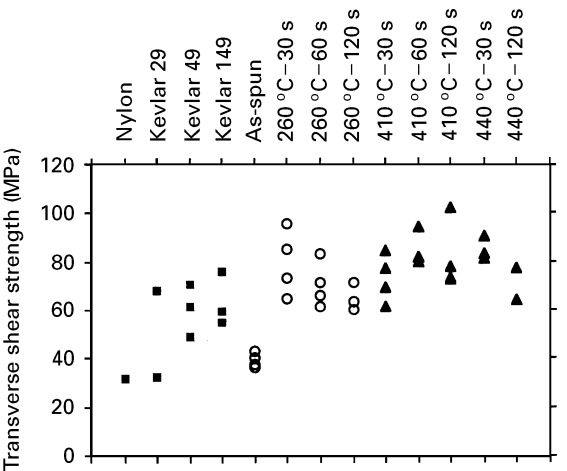

Figure 12 Plot of τ_{max} for various commercial fibres and for PPXTA fibres as-spun and heat-treated under tension at 260, 410 and 440 °C.

stands out due to its poor resistance to lateral deformation (low $\bar{\sigma}_p$, τ_{max}, W and high $\bar{\xi}_o$, at a given stress), which probably results from the lack of relatively strong hydrogen bonds between the molecules. On the other hand, nylon and Kevlar fibres have comparable transverse moduli indicating that the elastic modulus is little affected by the strength of intermolecular bonding. No major difference between the properties of Kevlar PPTA and of PPXTA heat-treated at 260 °C is detected.

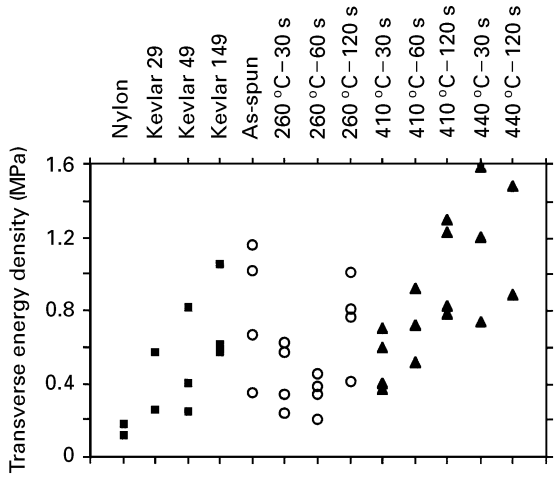

Figure 13 Plot of W for various commercial fibres and for PPXTA fibres as-spun and heat-treated under tension at 260, 410 and 440 °C.

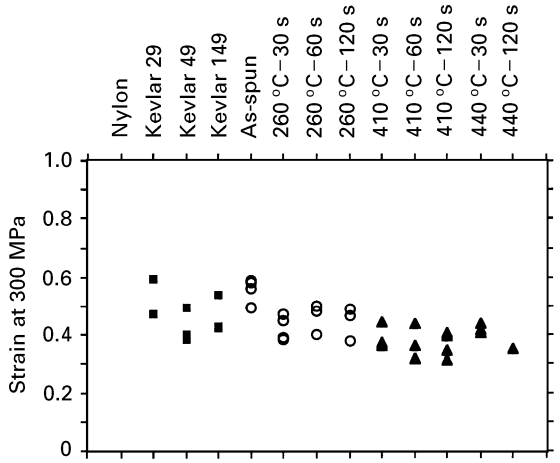

Figure 14 Plot of $\bar{\xi}_o$ at 300 MPa for various commercial fibres and for PPXTA fibres as-spun and heat-treated under tension at 260, 410 and 440 °C.

Comparison of PPXTA fibres as-spun and heat-treated at 260 °C shows the importance of a heat-treatment for the transverse deformation behaviour. The as-spun PPXTA fibres typically exhibit poor transverse properties, especially for the transverse elastic modulus E_t and for the transverse shear strength τ_{max}. The higher void content and the lesser orientation and crystallinity of as-spun fibres compared with heat-treated PPXTA fibres may be responsible for the poor deformation behaviour. In contrast, W is high, indicating that as-spun fibres store large energy or display large strains when the deformation becomes non-linear.

Given the experimental errors it is not possible to show trends for the transverse modulus E_t and shear strength τ_{max} of heat-treated PPXTA. However, the transverse elastic energy density W, critical strain $\bar{\sigma}_p$, and strains $\bar{\xi}_o$ at various stresses change with higher temperature and time of heat treatment. $\bar{\sigma}_p$ is highest for the cross-linked materials heat-treated at 410 °C or above which indicates that cross-linking delays the onset of local plasticity. W also increases with heat-treatment temperature which indicates that the

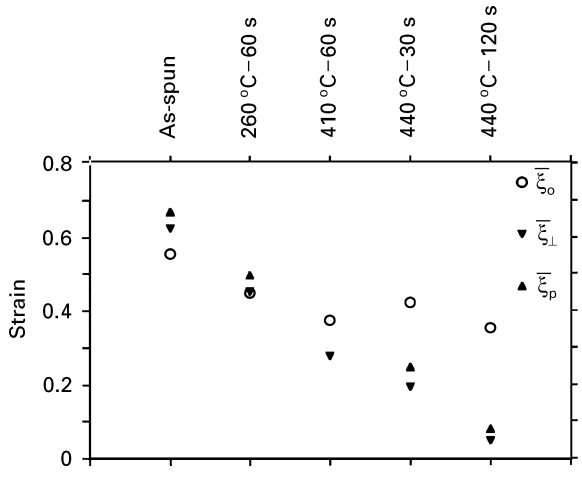

Figure 15 Plot of (○) $\bar{\xi}_o$ at 300 MPa, (▼) $\bar{\xi}_\perp$ after removal of a 300 to 370 MPa stress, (▲) $\bar{\xi}_p$ obtained from the pipette test using a 100 g load, for various PPXTA fibres. $\bar{\xi}_o$ is an elastic and plastic strain measured parallel to the load axis, $\bar{\xi}_\perp$ is a plastic strain measured perpendicular to the load axis, and $\bar{\xi}_p$ is a plastic strain measured perpendicular to the load axis with the pipette test.

cross-linked fibres store more energy during elastic deformation up to the proportional limit. The strains $\bar{\xi}_o$ at 100, 200 and 300 MPa are lowest for the cross-linked materials. Even though the amount of deformation decreases with density of cross-links or heat-treatment temperature and time, the effect does not seem as pronounced as the effect seen by Jiang *et al.* [29] with the pipette test for PPXTA fibres heat-treated at 330 °C for 60 and 120 s. It is important to note that the PPXTA fibres heat-treated at high temperature (410 and 440 °C) may undergo some degradation in addition to cross-linking and ordering [38]. The effect of cross-linking and of degradation is difficult to separate. One might expect a better resistance to lateral deformation in a cross-linked, yet not degraded, fibre.

The widths $d_\perp$ (width perpendicular to the loading direction) of the fibre samples compressed transversely up to 300 to 370 MPa were measured with the optical microscope. An apparent plastic strain $\bar{\xi}_\perp$ was calculated as $\bar{\xi}_\perp = (d_\perp - d)/d$. Fig. 15 compares $\bar{\xi}_\perp$ and $\bar{\xi}_o$ at 300 MPa for Kevlar 49 and PPXTA as-spun and heat-treated at 260, 410 and 440 °C. Evidently, cross-linking PPXTA does not modify $\bar{\xi}_o$ much but dramatically decreases $\bar{\xi}_\perp$. The PPXTA fibres heat-treated at 440 °C for 30 s were only slightly permanently deformed. The deformation zone of the equivalent fibres heat-treated for 120 s could barely be detected with optical microscopy. In this case, the length of the flattened region l could not be measured with the profile projector but was taken as the average of the measured length on other samples, for this particular alignment and glass punch.

The strain $\bar{\xi}_p$ obtained from the pipette test is similar to $\bar{\xi}_\perp$, since both are plastic strains measured perpendicular to the loading direction after unloading. Fig. 15 also illustrates the changes of $\bar{\xi}_p$ for various PPXTA fibres and for Kevlar 49. The similarity between $\bar{\xi}_p$ and $\bar{\xi}_\perp$ is obvious. Thus, applying a load of 100 g with a pipette of 7.25 mm in diameter gives the

same deformation as applying a load of 1000 g with a 2 mm flat punch, corresponding to a stress $\bar{\sigma}$ of 300 and 370 MPa. This equivalence may not hold for different materials and fibre diameters. Nevertheless, it is possible to get a well-controlled and reproducible lateral deformation state by compressing a sample between a glass slide and a glass pipette. The implication is that a variable as important as the plastic strain can be reliably and reproducibly estimated with a test as simple, quick and inexpensive as the pipette test.

The difference between measuring a deformed diameter $d_\perp$ after the test and measuring a displacement u during the test are first, that the stress is applied or not during the measurement, second, that the displacement corresponds to an expansion perpendicular to the loading direction or a contraction in the loading direction. The strain $\bar{\bar{\xi}}_o$ measured with the ITS machine is the elastic and plastic strain in contraction, whereas the strains $\bar{\bar{\xi}}_\perp$ and $\bar{\bar{\xi}}_p$ measured with the optical microscope are solely plastic in expansion. One explanation for the different results is that whereas samples heat-treated at 260 °C plastically deform, samples heat-treated at 440 °C elastically deform even at stresses around 300 to 370 MPa, much higher than the proportional limit stress $\bar{\sigma}_p$. This results from the heterogeneity of the stress within the cylindrical fibre. Thus the predominant effect of cross-linking appears to be to delay the onset of plastic deformation. The deviation from linearity in the transverse deformation behaviour most likely corresponds to global yielding for uncross-linked PPXTA but only to local yielding for cross-linked PPXTA. While the large strain ($\approx$40%) response of uncross-linked PPXTA is plastic or permanent, the cross-linked PPXTA exhibits a large strain recoverable response reminiscent of an elastomer.

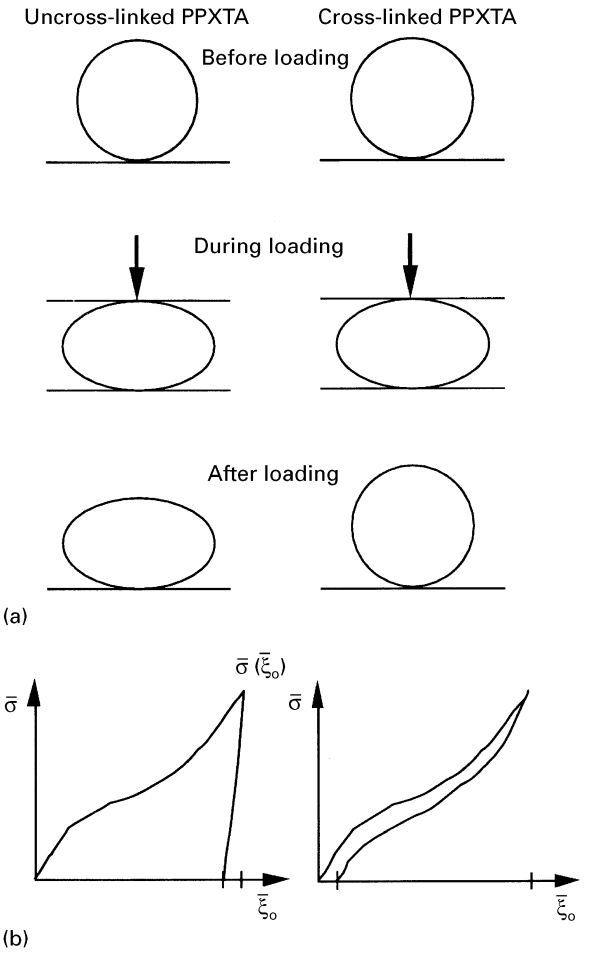

Figure 16 (a) Schematic of uncross-linked and cross-linked PPXTA fibres before, during and after transverse compressive loading. (b) Schematics of the predicted stress–strain curves during loading and during unloading.

It would be interesting in future work to record the unloading stress–strain curves after various applied peak stresses, and measure the extent of deformation after unloading. This discussion is summarized in Fig. 16. Schematics of uncross-linked and cross-linked PPXTA fibres before, during and after transverse compressive loading are displayed, together with schematics of the predicted stress–strain curves during loading and unloading. Phoenix and Skelton [15], Kawabata [19], and Knoff [20] only measure the transverse modulus and the stress at yield or the shear strength. Our study demonstrates the importance of additionally measuring the plastic and hysteresis behaviour by recording the unloading stress–strain curve, or by using the pipette test. Examining the plasticity might be particularly important for Knoff's study [20] of PPTA fibres of various water contents.

To summarize, the torsional and transverse modulus of PPXTA fibres do not vary much with the degree of cross-linking. The torsional modulus increases only by 13% as a result of cross-linking. The torsional modulus or $G_{\theta z}$ is a function of conformational rigidity, intermolecular interaction and fibre morphology. Torsion of the fibre involves intermolecular shear within the crystallites, between the crystallites, and between the microfibrils. Similarly, the transverse modulus is a function of intermolecular interaction and fibre morphology. The elastic lateral compression involves intermolecular compression, tension and shear at all levels of the morphology. The fibres are especially non-homogeneous when cross-linked since it is possible that the microfibrils are not cross-linked to one another as a result of the void area between them. In other words, there may be planes or regions of uncross-linked material, which may correspond to the interfibrillar space. Thus in the cross-linked materials, the applied torsion might be accommodated by interfibrillar shear. The same reasoning may be held for the applied lateral compression. This would explain the lack of a significant increase in the torsional and transverse modulus of cross-linked PPXTA, not predicted by molecular simulations.

As was discussed earlier, the state of stress in the laterally deformed fibres is non-homogeneous. The effect of cross-linking seems to delay the onset of plastic deformation, after deviation from linearity is observed in the stress–strain curves. A 300 to 370 MPa stress approximately induces a 40% plastic strain in uncross-linked PPXTA and a 40% recoverable strain in cross-linked PPXTA. A WAXD experiment was performed on PPXTA fibres heavily deformed between a glass pipette and a glass slide. Fig. 17 displays the diffraction patterns of PPXTA

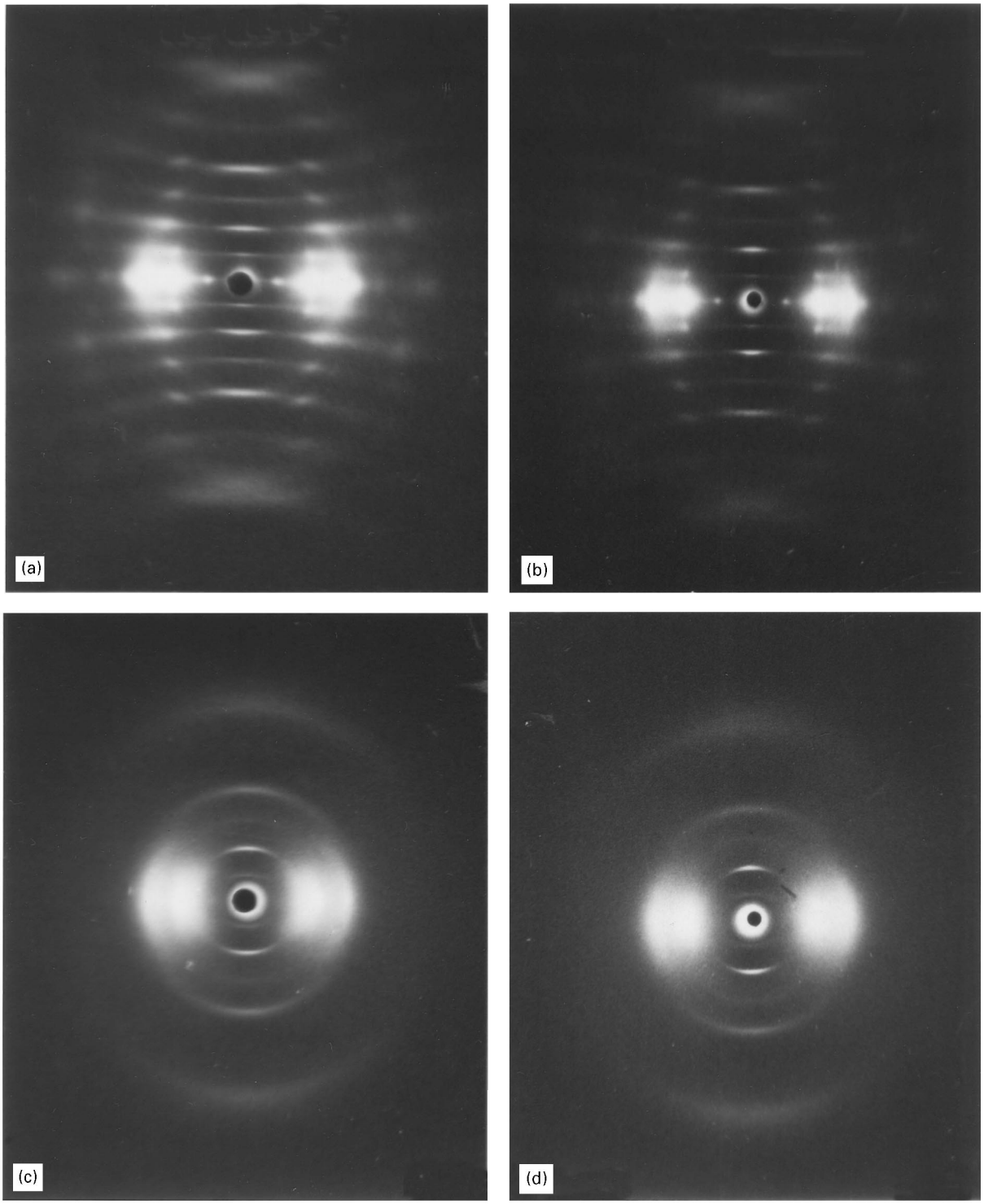

Figure 17 WAXD patterns of PPXTA heat-treated at (a) 260 °C and (b) 400 °C, (c) before and (d) after heavy lateral deformation.

heat-treated at 260 °C and 400 °C, before and after deformation. Equatorial scans are shown in Fig. 18. The appearance of the WAXD patterns of the deformed fibres suggests that the crystallites have been broken down resulting in spot broadening. However, the equatorial scans show that this apparent spot broadening is primarily a result of the misorientation resulting from the deformation. An interesting observation is the disappearance of the (1 0 0) reflections after deformation of both uncross-linked and cross-linked PPXTA. The loss of the (1 0 0) periodicity necessarily results from the BCB units becoming randomly oriented [28]. Thus heavy lateral deformation disrupts the preferential segregation of the BCBs in (1 0 0) planes. This disruption of the (1 0 0) symmetry cannot be accounted for only by shear on (2 0 0) hydrogen-bonded planes, but necessitates shear at an angle to the (2 0 0) planes, i.e. on other ($h\,k\,0$) planes. These results show that deformation takes place at the local unit cell level even in cross-linked materials.

Finally, this study of the transverse and torsional deformation behaviour of cross-linkable PPXTA

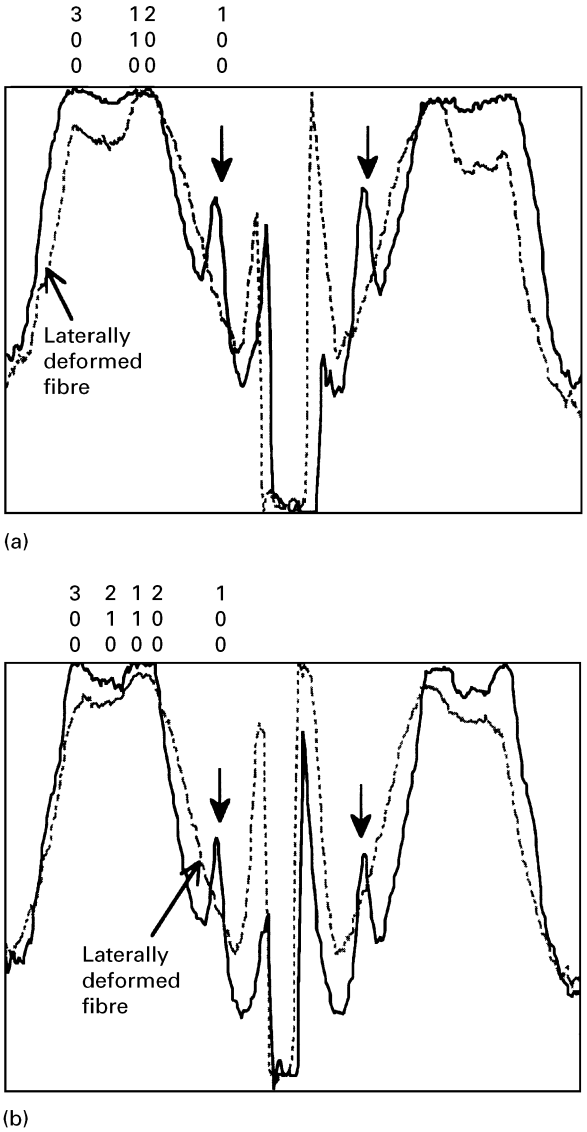

Figure 18 Equatorial scans of the WAXD of PPXTA heat-treated at (a) 260 °C and (b) 400 °C, before and after heavy lateral deformation.

allows a better understanding of the micromechanisms of kinking in extended-chain polymers. Lateral compression of the fibres involves shear deformation on ($h\,k\,0$) planes in the a or b direction, with c being the molecular and fibre axis direction. The transverse experiments basically show that cross-linking the PPXTA fibres increases the resolved shear stress on the ($h\,k\,0$) [1 0 0] or ($h\,k\,0$) [0 1 0] systems. Both the transverse and torsional experiments indicate that the cross-links little affect the shear or transverse stiffness. If the formation of kinks upon axial compression also involves shear of the ($h\,k\,0$) planes, albeit in the [0 0 1] direction, the kinking behaviour should be modified by the cross-links. Indeed we have shown elsewhere [48] that the energy to kink formation is higher in the cross-linked PPXTA system and that cross-linking may induce a transition in compressive failure from kinking to material rupture. Thus, the kink band formation necessitates intermolecular shearing and can be obstructed by raising the yield stress in shear via the incorporation of lateral covalent intermolecular cross-links.

5. Conclusions

Carbon and alumina fibres exhibit a brittle behaviour during lateral compression and display a very high modulus, whereas organic fibres exhibit a non-linear transverse deformation behaviour indicative of ductility. The laterally compressed surface of uncross-linked PPXTA was smooth, but numerous longitudinal cracks were observed for the cross-linked PPXTA fibres. In addition, the deformation zone of highly cross-linked PPXTA was almost not detectable, suggesting that these cross-linked fibres did not remain permanently deformed.

The as-spun PPXTA fibres display a low transverse modulus and transverse shear strength compared with the heat-treated fibres. However the lack of heat treatment in as-spun fibres does not seem to affect the torsional modulus and transverse elastic energy density. The transverse critical stress and elastic energy density at the proportional limit are highest for the cross-linked PPXTA fibres, suggesting that cross-linking delays the onset of plastic deformation and increases the energy stored during the deformation up to non-linear transverse deformation. The changes of the transverse modulus and shear strength of PPXTA with cross-linking were not experimentally significant. The transverse and shear modulus may be slightly higher for PPXTA than for Kevlar (PPTA). Yet, no major differences between the properties of Kevlar and of PPXTA heat-treated at 260 °C are detected.

The transverse compressive strain measured during loading decreases slightly with the cross-link density or with increased heat-treatment temperature, whereas the lateral plastic strain measured after unloading decreases dramatically with cross-link density. This suggests that at stresses of 300 to 370 MPa, above the proportional limit stress, the uncross-linked PPXTA fibres deform plastically ($\approx$40% strain) in a manner similar to PPTA, whereas the cross-linked PPXTA fibres deform elastically ($\approx$40% strain). This large strain non-linear elastic response is unique to the cross-linked PPXTA fibres and is reminiscent of the deformation behaviour of an elastomer.

Our study demonstrates the importance of evaluating the plastic and hysteresis deformation behaviour in addition to measuring the modulus and the stress at the proportional limit. An estimate of the lateral plastic strain may be obtained with a test as simple and inexpensive as the pipette test. Compressing a PPTA or PPXTA fibre between a 7.25 mm diameter cylindrical pipette and a flat substrate with a 100 g load generates roughly the same plastic deformation as applying a 300 to 370 MPa apparent stress on the fibre between two flat parallel platens, or applying a 1 kg load through a flat 2 mm wide punch.

Since cross-linking obstructs both transverse plastic deformation and kink band formation [48], the formation of kink bands upon axial compression must involve a deformation mechanism similar to the plastic shear deformation during transverse compression.

Acknowledgements

This research was supported by the US Army Advanced Concept Technology Committee (DAAK6-92-

K-0005). Generous support was also provided from DuPont, Hoechst-Celanese, and the NSF National Young Investigator Program (NSF-DMR-9257560). The authors acknowledge Steve Allen and Warren Knoff for helpful discussions, Robert Irwin for spinning our polymer, and the High Temperature Material Laboratory of Oak Ridge National Laboratories for providing the interfacial test system machine. The use of the interfacial test system at Oak Ridge National Laboratory was possible thanks to the support from the US Department of Energy, Assistant Secretary for Energy Efficiency and Renewable Energy, Office of Industrial Technologies, Industrial Energy Efficiency Division and Continuous Fibre Ceramic Composites Program and by the US Department of Energy, Assistant Secretary for Energy Efficiency and Renewable Energy, Office of Transportation Technologies as Part of the High Temperature Materials Laboratory User Program under contract DE-AC05-96OR22464 with Lockheed Martin Energy Research Corporation. MCGJ also thanks Wright Patterson Air Force Base for the use of their flat-film X-ray camera.

References

1. H. H. YANG, "Aromatic high-strength fibres" (Wiley-Interscience, New York, 1989).
2. S. R. ALLEN, *J. Mater. Sci.* **22** (1987) 853.
3. S. J. DETERESA, S. R. ALLEN and R. J. FARRIS, in "Composite applications: the role of matrix, fiber, and interface" edited by T. Vigo and B. Kinzig (VCH Publishers, New York, NY, 1992) Chapter 4.
4. C. Y.-C. LEE and U. SANTHOSH, *Polym. Engng Sci.* **33** (1993) 907.
5. D. L. VEZIE, Ph.D. Dissertation, Massachusetts Institute of Technology, Cambridge, MA (1993).
6. D. C. MARTIN, Ph.D. Dissertation, The University of Massachusetts, Amherst, MA (1990).
7. D. C. MARTIN and E. L. THOMAS, *J. Mater. Sci.* **26** (1991) 5171.
8. V. I. VLADIMIROV, A. G. ZEMBIL'GOTOV and N. A. PERTSEV, *Fiz. Tverd. Tela* (*Leningrad*) **31** (1989) 233.
9. M-C. G. JONES and D. C. MARTIN, *Macromolecules* **28** (1995) 6161.
10. S. R. ALLEN and E. L. ROCHE, *Polymer* **30** (1989) 996.
11. M. G. NORTHOLT and R. V. D. HOUT, *ibid.* **26** (1985) 310.
12. W. F. KNOFF, *J. Mater. Sci. Lett.* **6** (1987) 1392.
13. S. R. ALLEN, Ph.D. Dissertation, University of Massachusetts, Amherst, MA, (1983).
14. P. MASON, *Textile Res. J* **34** (1964) 1104.
15. S. L. PHOENIX and J. SKELTON, *ibid.* **44** (1974) 934.
16. D. W. HADLEY, I. M. WARD and J. WARD, *Proc. Roy. Soc. A* **1401** (1965) 275.
17. S. K. BATRA and N. SYED, *J. Polym. Sci. Polym. Phys.* **13** (1975) 369.
18. S. A. JAWAD and I. M. WARD, *J. Mater. Sci.* **13** (1978) 1381.
19. S. KAWABATA, *J. Textile Inst.* **81** (1990) 432.
20. W. F. KNOFF, in "Basic properties of fibers and fiber assemblies, performance and design of new fibrous materials," Proceedings of the 21st Textile Research Symposium, Mt. Fuji Educational Training Center, Susono City, Shizuoka, Japan, 7–9th August (1992).
21. T. KOTANI, J. SWEENEY and I. M. WARD, *J. Mater. Sci.* **29** (1994) 5551.
22. S. J. DETERESA, S. R. ALLEN, R. J. FARRIS and R. S. PORTER, *ibid.* **19** (1984) 57.
23. S. R. ALLEN, *Polymer* **29** (1988) 1091.
24. S. J. DETERESA, R. S. PORTER and R. J. FARRIS, *J. Mater. Sci.* **23** (1998) 1886.
25. V. R. MEHTA and S. KUMAR, *ibid.* **29** (1994) 3658.
26. L. J. MARKOSKI, K. A. WALKER, G. A. DEETER, G. E. SPILMAN, D. C. MARTIN and J. S. MOORE, *Chem. Mater.* **5** (1993) 248.
27. G. E. SPILMAN, L. J. MARKOSKI, K. A. WALKER, G. A. DEETER, D. C. MARTIN and J. S. MOORE, *Polym. Mater. Sci. Engng* **68** (1993) 139.
28. M-C. G. JONES, T. JIANG and D. C. MARTIN, *Macromolecules* **27** (1994) 6507.
29. T. JIANG, J. RIGNEY, M-C. G. JONES, L. J. MARKOSKI, G. E. SPILMAN, D. F. MIELEWSKI and D. C. MARTIN, *ibid.* **28** (1995) 3301.
30. W. WANG, W. RULAND and Y. COHEN, *Acta Polymer* **44** (1993) 273.
31. Y. COHEN, H. H. FROST and E. L. THOMAS, in "Reversible polymeric gels and related systems", edited by P. S. Russo (American Chemical Society Symposium Series, Washington DC, 1987) Chapter 12.
32. M. G. NORTHOLT, *Eur. Polym. J.* **10** (1974) 799.
33. M. G. DOBB, in "Handbook of Composites, Vol. 1, Strong Fibres", edited by W. Watt and B. V. Perov (Elsevier Science Publishers, Amsterdam, 1985).
34. H. ADE and B. HSIAO, *Science* **262** (1993) 1427.
35. L. FRYDMAN, unpublished research (1994).
36. M. J. MARKS, *Polymer Preprints* **66** (1992) 362.
37. M. J. MARKS, J. S. ERSKINE and D. A. McCRERY, *Macromolecules* **27** (1994) 4114.
38. D. F. MIELEWSKI, D. C. MARTIN and D. R. BAUER, *Polymer Materials Science and Engineering* **71** (1994) 160.
39. S. L. MAYO, B. D. OLAFSON and W. A. GODDARD, *J. Phys. Chem.* **94** (1990) 8897.
40. G. E. SPILMAN, T. JIANG, J. S. MOORE and D. C. MARTIN, *Polymer Preprints* **35**(2) (1994) 667.
41. W. C. OLIVER and G. M. PHARR, *J. Mater. Res.* **7** (1992) 1564.
42. M. K. FERBER, E. LARA-CURZIO, A. A. WERESZCZAK and R. A. LOWDEN, *Measurement Sci. Technol.* (1997) in press.
43. A. A. WERESZCZAK, M. K. FERBER and R. A. LOWDEN, *Ceram. Eng. Sci. Proc.* **14** (1993) 156.
44. P. M. CUNNIFF, private communication (1994).
45. V. R. MEHTA and S. KUMAR, *J. Mater. Sci.* **29** (1994) 3658.
46. R. J. SCHADT, E. J. CAIN, K. H. GARDNER, V. GABARA, S. R. ALLEN and A. D. ENGLISH, *Macromolecules* **26** (1993) 6503.
47. R. J. SCHADT, K. H. GARDNER, V. GABARA, S. R. ALLEN, D. B. CHASE and A. D. ENGLISH, *ibid.* **26** (1993) 6509.
48. M-C. G. JONES and D. C. MARTIN, *J. Mater. Sci.* (1997) in press.

Received 17 July
and accepted 23 October 1996